



Contents lists available at ScienceDirect

## Dyes and Pigments

journal homepage: [www.elsevier.com/locate/dyepig](http://www.elsevier.com/locate/dyepig)

## Self-assembly, optical and electrical properties of five membered O- or S-heterocyclic annulated perylene diimides

Yongshan Ma<sup>a, b, c</sup>, Zhiqiang Shi<sup>a, \*</sup>, Andong Zhang<sup>a</sup>, Jiaofu Li<sup>a</sup>, Xiaofeng Wei<sup>b, c</sup>, Tianyi Jiang<sup>b, c</sup>, Yanan Li<sup>a</sup>, Xiaolei Wang<sup>a</sup>

<sup>a</sup> College of Chemistry, Chemical Engineering and Materials Science, Collaborative Innovation Center of Functionalized Probes for Chemical Imaging in Universities of Shandong, Shandong Normal University, Jinan 250014, PR China

<sup>b</sup> School of Municipal and Environmental Engineering, Shandong Jianzhu University, Jinan, PR China

<sup>c</sup> Co-Innovation Center of Green Building, Jinan 250101, PR China

## ARTICLE INFO

## Article history:

Received 28 March 2016

Received in revised form

16 June 2016

Accepted 18 June 2016

Available online xxx

## Keywords:

Heterocyclic annulated perylenes

Self-assembly

Nanostructure

Density functional theory calculations

X-ray diffraction analysis

## ABSTRACT

In this work, a new asymmetrically five-membered O-heterocyclic annulated perylene diimide (O-PDI) has been synthesized. The compounds O-PDI and asymmetrically five-membered S-heterocyclic annulated perylene diimide (S-PDI) self-assembled into nanoneedle and nanosheet, respectively. Photo-physical, electrochemical and thermal properties were investigated by UV–vis absorption, fluorescence, cyclic voltammetric, thermogravimetric and differential scanning calorimetry techniques. Optical, fluorescence, scanning and transmission electron microscopies were employed in the molecular self-assembly studies. Due to significant electronic coupling between their heteroatom/heterocycles and perylene diimide (PDI) cores, the intermolecular  $\pi$ - $\pi$  actions are neglectable, providing high luminescence efficiency. At the same time, the space between perylene chromophores is still very short (3.3 Å for O-PDI and 3.23 Å for S-PDI), which is favorable for the hopping transportation of charge carrier from one molecule to a neighboring one. These compounds could be candidate materials for acquiring well defined organic nanostructures with both excellent charge-transporting and good light-emitting capabilities.

© 2016 Elsevier Ltd. All rights reserved.

### 1. Introduction

During the last years, self-organization has been forecasted to be a tool for the synthesis of well defined organic nanostructures and has received increased attention [1–3]. Perylene dyes were extensively studied due to their good properties such as excellent photostabilities and high fluorescence quantum yields [4–8]. As an alternative of carbon nanotubes and other inorganic semiconductor nanowires, perylene-3,4,9,10-tetracarboxylic bisimides (PDIs) can be potentially used for low-cost processes such as spin-coating, evaporating and printing [9,10].

During the search of high performance organic semiconductors for molecular devices, fused and extended heteroarenes are recognized as one of the most promising molecular scaffolds [11]. The introduction of heterocycles or heteroatoms to a  $\pi$ -conjugated system is a facile approach for the construction of intramolecular charge transfer compounds, with the lone pairs of electrons of the

heteroatoms being used as electron donors [12]. Incorporating heteroatoms into the perylene skeleton can dramatically change the electronic structures and photochemical properties of these heterocyclic annulated perylenes [13]. Extension along the short molecular axis always causes a hypsochromic shift [14]. Furthermore, highly  $\pi$ -extended heteroarenes would also induce a variety of intermolecular interactions, such as van der Waals interactions and heteroatom-heteroatom interactions. These interactions are essential to achieve highly ordered supramolecular self-assembled structure, which then results in excellent device performance [15]. Current reports on annulation of PDIs with heterocycles in one bay region have focused on their synthesis and optical properties. Heinz Langhals synthesized five membered S-heterocyclic annulated perylene diimide (S-PDI) by reaction of the mono-substituted nitroperylene bisimide with sulfur in DMF or NMP. The UV/Vis spectra exhibits a hypsochromic shift of 12 nm compared to PDI. The fluorescence quantum yield is 71% in solution and there is an intense solid-state fluorescence [16]. Li Yuliang and coworkers developed new methods to synthesize two N-heterocyclic annulated perylene diimides. These N-heterocycle-annulated PBIs exhibit distinct optical and electronic properties because of

\* Corresponding author.

E-mail address: [zshi@sdsnu.edu.cn](mailto:zshi@sdsnu.edu.cn) (Z. Shi).

significant electronic coupling between their heteroatom/heterocycles and PDI cores [17].

In this work, a new heterocyclic annulated perylene diimides: asymmetrically five-membered O-heterocyclic annulated perylene diimide (O-PDI) (Scheme 1) has been synthesized. We report O-PDI and S-PDI derivative that lack flexible solubilizing groups in the molecular structure, and demonstrate their self-assembly into nanoneedle and nanosheet, respectively. Their optical, electrical and thermal properties were also assayed. Through the analysis of their crystal structures, the effect of heterocyclic substituents on the electronic and optical properties of perylene diimide was investigated. Because of significant electronic coupling between their heteroatom/heterocycles and PDI cores, the dimers of O-PDI or S-PDI adopted a similar slipped  $\pi$ -stacked packing motif between neighboring molecules that restricted the intermolecular  $\pi$ - $\pi$  stacking. The heteroatom actually help firming up the stacking of the molecules through non-covalent interactions, and electrostatic attraction between the electron-rich atom O/S and electron-poor perylene core. PDIs are among the most insoluble organic pigments and their processing into nanostructures by self-assembly protocols in solution has so far only been accomplished for derivatives bearing long n-alkyl side chains or basing on large  $\pi$ -scaffold contortion [18]. This study will be helpful for exploring feasible routes to acquire well defined organic nanostructures. Furthermore, such molecular tailoring approach would help to design and synthesize novel organic semiconductive materials with both excellent charge-transporting and good light-emitting capabilities.

## 2. Experimental section

### 2.1. Materials

All chemical reagents were of reagent grade and purchased from commercial source. They were purified through conventional procedures prior to use. *N, N'*-dicyclohexyl-3,4,9,10-tetracarboxylic acid bisimide **1** and *N, N'*-dicyclohexyl-1-nitroperylene-3,4,9,10-tetracarboxylic acid bisimide **2** were synthesized according to the literature procedure [19,20].

### 2.2. Synthesis

#### 2.2.1. Synthesis of compound O-PDI

Compound **2** (120 mg, 0.2 mmol) was dissolved in *N*-

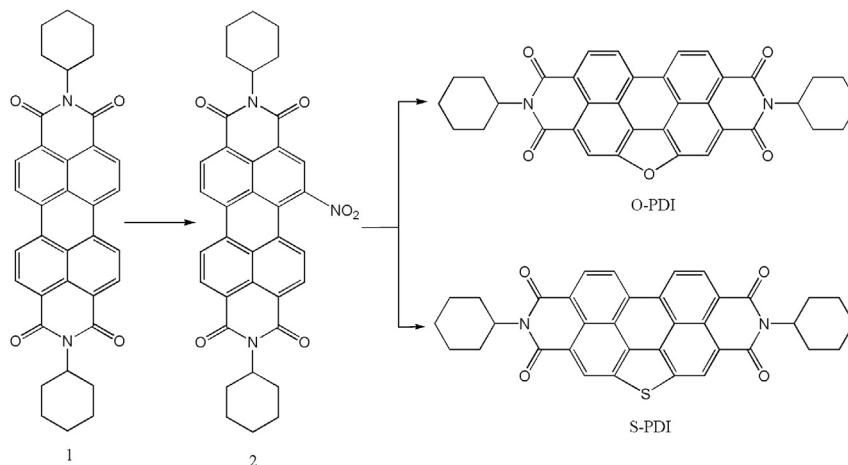
methylpyrrolidone (NMP, 10 ml). The resulting solution was stirred at 180 °C under O<sub>2</sub> for 5 h until the starting material could not be detected by TLC, and then poured into 100 ml of 2 M HCl. The precipitate was collected by vacuum filtration and washed with water. After solvent was removed under vacuum, the crude product was purified by silica gel column chromatography with eluent dichloromethane/petroleum ether (5/2). After solvent was removed, a bright yellow solid of 34 mg (30%) O-PDI was obtained. <sup>1</sup>H NMR (CHCl<sub>3</sub>, TMS, ppm):  $\delta$  = 8.95 (d, 2H), 8.83 (d, 4H), 5.16 (m, 2H), 2.66–2.63 (m, 4H), 1.94–1.55 (m, 8H), 1.41–1.26 (m, 8H). <sup>13</sup>C NMR (75 MHz, CDCl<sub>3</sub>, ppm):  $\delta$  = 164.78, 163.74, 154.15, 133.93, 130.38, 126.46, 125.03, 124.36, 119.34, 54.50, 29.27, 26.65, 25.48. FT-IR (KBr, cm<sup>-1</sup>):  $\nu$  = 2922, 1689, 1649, 1611, 1415, 1341, 1307, 1259, 1179, 1000, 896, 852, 805, 735, 628, 576, 449, 416. MS (APCI): *m/z* 568.1947 M<sup>-</sup>.

#### 2.2.2. Synthesis of compound S-PDI

The compound S-PDI was synthesized according to the literature procedure [16]. Briefly, 180 mg (0.3 mmol) compound **2** and 160 mg (5.0 mmol) powdered sulfur reacted for 12 h in NMP at 130 °C under argon atmosphere to yield S-PDI in 32%. <sup>1</sup>H NMR (CHCl<sub>3</sub>, TMS, ppm):  $\delta$  = 9.31 (s, 2H), 8.96 (d, 2H, *J* = 8.1 Hz), 8.90 (d, 2H, *J* = 8.1 Hz), 5.17 (m, 2H), 2.66 (m, 4H), 1.94 (m, 4H), 1.84 (m, 6H), 1.47–1.38 (m, 6H). FT-IR (KBr, cm<sup>-1</sup>):  $\nu$  = 2917, 1698, 1648, 1593, 1426, 1349, 1303, 1234, 1175, 989, 889, 850, 803, 784, 735, 683, 628, 594, 449. MS (APCI): *m/z* 584.1729 M<sup>-</sup>.

### 2.3. Characterization and measurement

<sup>1</sup>H NMR and <sup>13</sup>C NMR spectra were recorded in CDCl<sub>3</sub> on a Bruker 300 MHz spectrometer. FT-IR spectrum were measured with Bruker Tensor-27 spectrophotometer. Mass spectra were recorded on a Bruker Maxis UHR-TOF mass spectrometer. UV-Vis absorption spectra and fluorescence measurements were recorded with a Varian CARY-50 spectrophotometer and a Hitachi FL-4500 spectrofluorometer, respectively. Cyclic voltammetry (CV) was performed with a CH 1604C electrochemical analyzer at a scan rate of 100 mV/s and the current sensitivity was given as 0.01  $\mu$ A by using three electrode cell units, polished 2 mm glassy carbon as working electrode, Pt as counter electrode and Ag/AgNO<sub>3</sub> as reference electrode by using. Tetrabutylammonium perchlorate (Bu<sub>4</sub>NClO<sub>4</sub>) was used as the supporting electrolyte. The optical microscopic images and fluorescence microscopic images were obtained with an Olympus (Japan) BH2 fluorescence microscope, which provides



**Scheme 1.** Synthesis route of symmetrically five-membered O-heterocyclic annulated perylene diimide (O-PDI) and asymmetrically five-membered S-heterocyclic annulated perylene diimide (S-PDI).

excitation in the range of 450–490 nm. Scanning electron microscopic (SEM) measurement was performed with a FEI NOVA NANOSEM 450 microscope. The sample was prepared by casting one drop of the nanorod suspension onto a glass coverslip. The dried sample was coated with gold prior to the SEM imaging. Transmission electron microscopic (TEM) was recorded using a JEOL instrument. Thermogravimetric analysis (TGA) was conducted with a TA Q50 instrument. Differential scanning calorimetry (DSC) measurements were performed using a Perkin-Elmer DSC-7 calorimeter. The sample temperature of TGA and DSC was maintained at 10 °C/min under a nitrogen atmosphere.

#### 2.4. Computation details

The Becke's three parameter gradient-corrected hybrid density function B3LYP method [21,22] and the standard 6-31G\* (d) basis set [23] were used for both structure optimization, the property calculations and the molecular arrangement in O-PDI/S-PDI solid based on two molecular models. All the calculations were performed using the Gaussian 03 program installed on a Windows PC.

### 3. Results and discussion

#### 3.1. Synthesis and characterization

Scheme 1 shows the chemical structures and synthetic routes of O-PDI and S-PDI. The synthesis started from an imidization of perylene bisanhydride by reaction with cyclohexylamine. The compound **2** was achieved by a reaction of compound **1** with

cerium (IV) ammonium nitrate ( $\text{Ce}(\text{NH}_4)_2(\text{NO}_3)_6$ ) and 96% nitric acid under ambient temperature in dichloromethane with a high yield (>90%). The compound S-PDI was synthesized according to a literature procedure [16]. Treatment of compound **2** with oxygen in air at 180 °C for 5 h directly afforded the bright yellow O-PDI. The structure of the compound O-PDI was fully characterized by different spectroscopic methods, including  $^1\text{H}$  and  $^{13}\text{C}$  NMR, FTIR and mass spectral techniques.

#### 3.2. Optical properties and self-assembled structures

The optical properties of heterocyclic annulated perylene diimides O-PDI and S-PDI in dichloromethane were investigated by UV–vis absorption (Fig. S-1a) and photoluminescence spectroscopy (Fig. S-1b), together that of unsubstituted perylene diimide **1** for comparison. The UV–vis absorption spectra showed that they all exhibit well-defined vibronic  $\pi$ – $\pi^*$  transition absorption bands with the longest maximum at 500 nm and 510 nm for S-PDI and O-PDI, respectively. They are all slightly blue-shifted relative to the corresponding parent compound perylene diimide ( $\lambda_{\text{max}} = 525$  nm) as a reflection of the extended aromatic core along the short molecular axis [14]. In comparison with S-PDI, the maximum absorption of O-PDI is bathochromically shifted about 10 nm. The fluorescence spectra depict the same structure with a mirror image of the absorption spectrum and the emission peaks are appeared at 522 nm and 515 nm for O-PDI and S-PDI, respectively. Moreover, the fluorescence spectra of O-PDI and S-PDI are also blue-shifted relative to that of compound **1**. Therefore, both the absorption and fluorescence spectra of the O-PDI and S-PDI are blue-shifted in

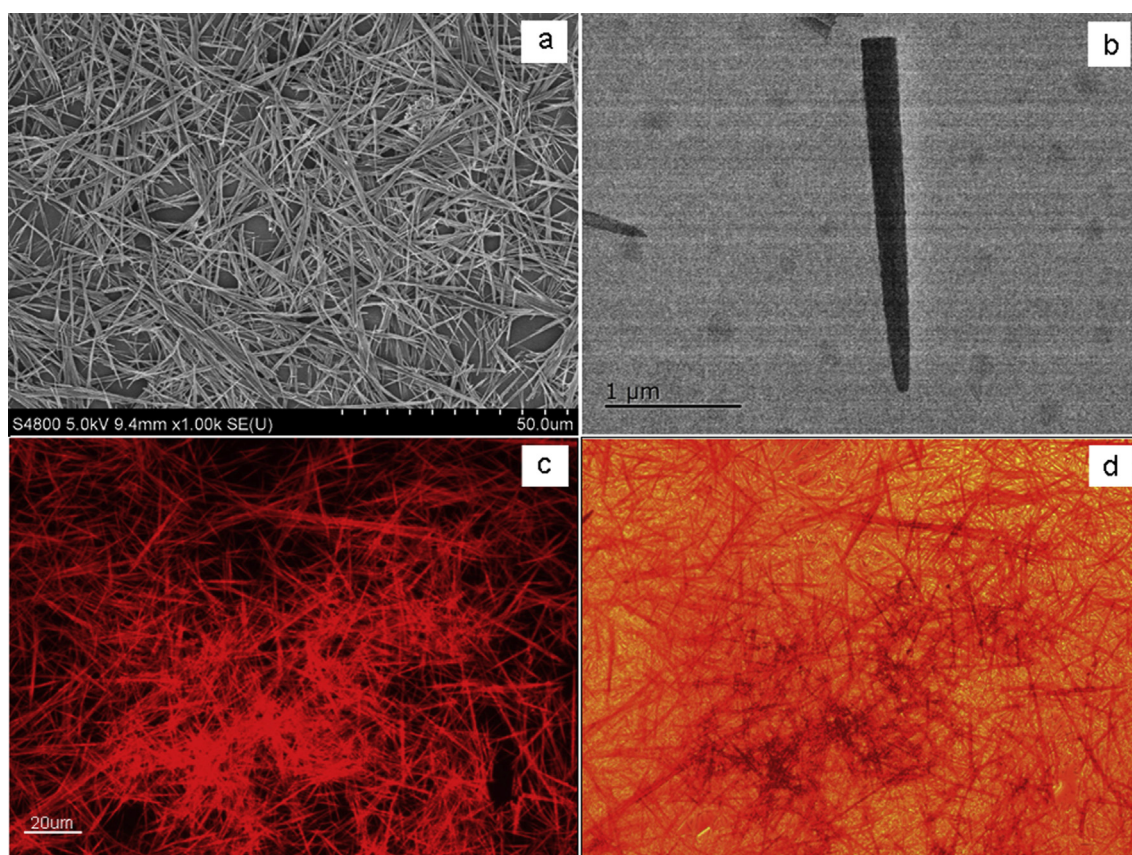


**Fig. 1.** Self-assembled structures of O-PDI nanoneedle deposited on a glass slide: (a) A large area SEM image. (b) TEM image. (c) Fluorescence microscopic image. (d) Optical microscopic image.

comparison with that of compound **1**. This means that the energy gap between the electronic excited state and the ground state of perylene bisimide can be turned by annulation the five membered O- or S- heterocycle into one bay region of perylene skeleton. The heteroatom annulated perylene diimides presented here possess small Stokes shifts of about 12 and 15 nm for O-PDI and S-PDI, respectively.

The UV–Vis absorption spectra and the fluorescence spectra of O-PDI and S-PDI in dichloromethane at various concentrations were shown in Figs. S-2 and S-3, respectively. Both the maximum absorbing and emissive wavelength ( $\lambda_{\max}$ ) are not shifted with variation of concentration. The spectra of O-PDI showed two absorption bands (510 nm, 476 nm) and a broad shoulder peak around 447 nm, which corresponding to the characteristics of the 0–0, 0–1, and 0–2 transition energy, and the absorption peaks of S-PDI appeared at 500, 467 and a shoulder around 439 nm. As free monomers, the normal progression of Franck–Condon factors was  $A^{0-0} > A^{0-1} > A^{0-2}$ . However, the 0–1 transition increases as the monomer begin to aggregate [24]. The 0–1 transition absorption of both O-PDI (from  $4 \times 10^{-6}$  to  $2 \times 10^{-5}$  M) and S-PDI (from  $5 \times 10^{-6}$  to  $4 \times 10^{-5}$  M) showed scarcely any increase in dichloromethane (Figs. S-2b and S-3b), suggesting that the  $\pi$ – $\pi$  interactions do not occur in higher concentration for O-PDI and S-PDI.

PDI derivatives other than alkylated PDI derivatives indicating extremely high solubility in organic solvents have recently been reported. For example, Masahiro Funahashi et al. have reported a solution-processable n-type PDI derivative bearing disiloxane chains. The Liquid-crystalline PDI derivative exhibits an ordered columnar phase at room temperature in which the electron mobility exceeds  $0.1 \text{ cm}^2 \text{ V}^{-1} \text{ s}^{-1}$  [25]. Both O-PDI and S-PDI have

significant electronic coupling between their heteroatom/heterocycles and PDI cores [26], and the cyclohexyl end-capping groups increase the steric bulkiness to the periphery of the two molecules [27]. So, despite the extension of the aromatic core of perylene, these two PDI derivatives are soluble in common organic solvents, and thus allowed us to compare their UV–Vis in a range of solvents (cyclohexane, ethylene acetate, tetrahydrofuran, dichloromethane and dimethylformamide) as shown in Fig. S-4. The shapes of spectra were similar in the solvents studied and the spectral shift was not straightly dependent on the solvent polarity. This may be due to some specific solvent-heteroatom interaction occurs for various solvents. To facilitate the molecular aggregation, we have used a mixture of solvents composed of dichloromethane and methanol. The process involves transferring a larger amount (1:2 volume) of methanol atop a concentrated dichloromethane solution of O-PDI/S-PDI in a glass vial. Within a few minutes, aggregates were formed at the interface. Figs. S-5 and S-6 shows the absorption spectral monitoring of the self assembling process of O-PDI and S-PDI. The absorption peak decreased gradually with time. This depicts the formation of nanocrystalline structures. Also we can see the absorption peak of O-PDI decreases more quickly than that of S-PDI. It can be attributed to the hydrogen bonding interaction between O and methanol.

Fig. 1a shows the SEM image of O-PDI nanostructures. Long flexible nanoneedles with uniform morphology in terms of both width and thickness can be seen. The average width is 200 nm, and the length is in the range within a few tens of micrometers (Fig. 1b). Fluorescence microscopic image of nanoneedles exhibits tapered, sharp ends (Fig. 1c). Optical microscopic image also supports the observed nanoneedle morphology (Fig. 1d). In contrast to O-PDI,

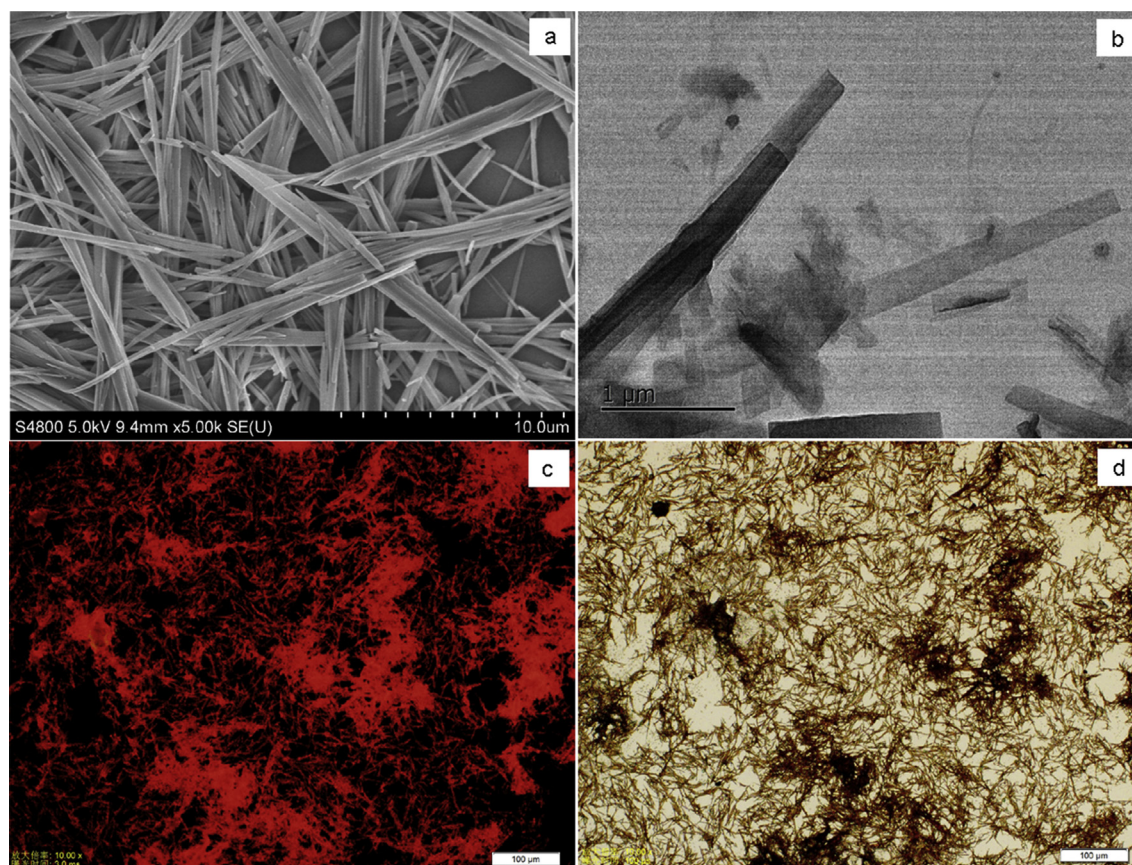
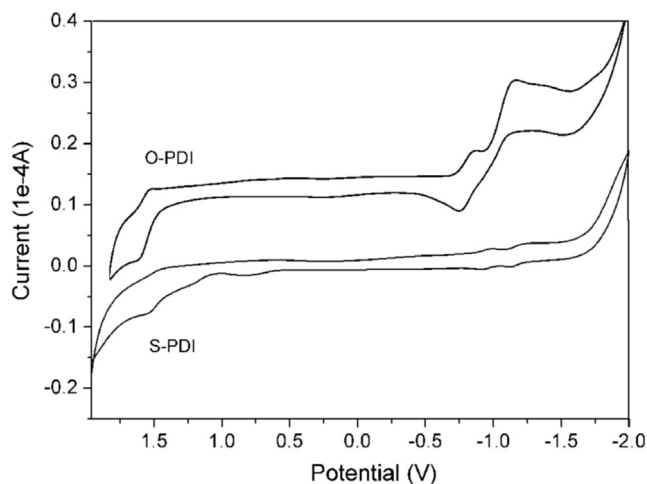


Fig. 2. Self-assembled structures of S-PDI nanosheet deposited on a glass slide: (a) A large area SEM image. (b) TEM image. (c) Fluorescence microscopic image. (d) Optical microscopic image.

the SEM image of the S-PDI shows that the molecules were assembled as 1D nanosheet (Fig. 2a), with an average width of 200 nm (Fig. 2b). The morphology was also supported by optical and fluorescence microscopic images (Fig. 2c and d). Fluorescence microscopic images of S-PDI nanosheet deposited on glass surface were recorded at 450–490 nm. The strong red emission was clearly seen in each nanosheet. Nanosheet bundle is also clearly seen in optical microscopic image (Fig. 2d). The optical microscopic measurements of O-PDI and S-PDI suggested the uniaxial crystal structure of the nanostructures.

### 3.3. Electrochemical and thermal properties of dyes

The cyclic voltammograms of O-PDI and S-PDI are illustrated in Fig. 3. When placed in dichloromethane and subjected to modest potentials, these chromophores undergo two quasi-reversible reductions and one quasi-reversible oxidation. These two quasi-reversible reduction processes originate from successive reduction of the imide groups to give a radical anion (O-PDI<sup>•-</sup> or S-PDI<sup>•-</sup>) in the first reduction step and a dianion (O-PDI<sup>2-</sup> or S-PDI<sup>2-</sup>) in the second step [5]. The first reduction process increases the electron density on the carbonyl oxygen of one imide group. The addition of a second electron to the opposite imide group is governed by two factors: one is the capability of delocalizing the surplus electron density imposed on the molecule during the first reduction step and other one is the coulombic repulsion between the introduced charges of the same sign. Table 1 summarizes the redox potentials and the highest occupied molecular orbital (HOMO) and the lowest unoccupied molecular orbital (LUMO) energy levels estimated from cyclic voltammetry (CV). It appears that both the first reduction and the first oxidation potentials of O-PDI are more positive than that of



**Fig. 3.** The cyclic voltammogram of O-PDI and S-PDI in CH<sub>2</sub>Cl<sub>2</sub> (under N<sub>2</sub> atmosphere, scanning rate 20 mV/s) using Bu<sub>4</sub>NPF<sub>6</sub> as electrolyte, glassy carbon electrode as work electrode, platinum as the counter electrode, and the Ag/AgNO<sub>3</sub> as the reference electrode.

**Table 1**

Cyclic voltammetry data and molecular orbital energies of O-PDI and S-PDI with respect to the vacuum level.

Molecule	E <sub>red1</sub> <sup>o</sup>	E <sub>red2</sub> <sup>o</sup>	E <sub>ox</sub> <sup>o</sup>	LUMO (eV) <sup>b</sup>	HOMO (eV) <sup>b</sup>	E <sub>gap</sub> (eV) <sup>b</sup>
O-PDI	-0.86	-1.17	1.62	-3.94	-6.42	2.48
S-PDI	-0.999	-1.23	1.551	-3.80	-6.35	2.55

<sup>a</sup> Measured in a solution of 0.1 M tetrabutylammonium hexafluorophosphate (TBAPF<sub>6</sub>) in dichloromethane versus Ag/AgNO<sub>3</sub> (in V).

<sup>b</sup> Calculated from E<sub>HOMO</sub> = -4.88 - (E<sub>oxd</sub> - E<sub>Fe/Fe+</sub>), E<sub>LUMO</sub> = E<sub>HOMO</sub> + E<sub>gap</sub>.

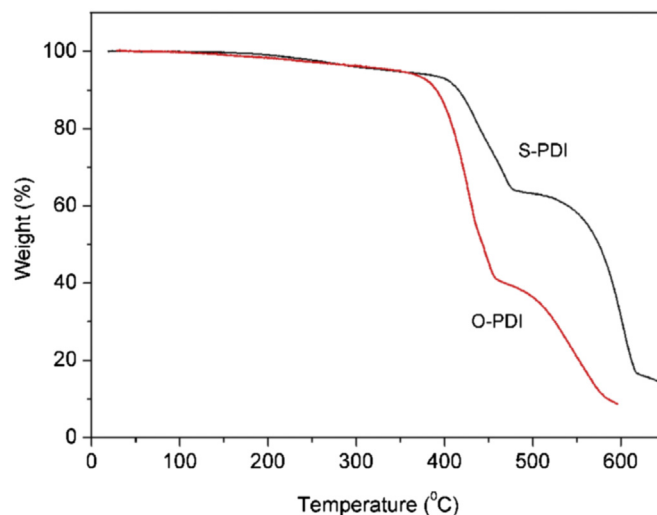


**Fig. 4.** Thermogravimetric analysis graphs for O-PDI (red line) and S-PDI (black line) in nitrogen atmosphere at normal pressure. Heating rate, 10 °C/min. (For interpretation of the references to colour in this figure legend, the reader is referred to the web version of this article.)

S-PDI, while both the HOMO and LUMO energy levels decrease with the trend. This can be explained by the fact that the O has better electron-withdrawing ability than the S. The HOMO/LUMO energy levels of O-PDI and S-PDI are estimated to be -6.42/-3.94 and -6.35/-3.80 eV, respectively.

The thermal properties of O-PDI and S-PDI were investigated by thermogravimetric analysis (TGA) and differential scanning calorimetry (DSC). The decomposition temperature of O-PDI is 370 °C and that of S-PDI is 400 °C; this shows that the S-PDI is more thermally stable than the O-PDI (Fig. 4). DSC analysis of O-PDI and S-PDI showed two endothermic peaks at 31, 85 °C and 21, 30 °C upon heating, respectively (Fig. 5). It was found that both of the O-PDI and S-PDI exhibit no glass transition temperature during DSC running up to 220 °C.

### 3.4. X-ray diffraction study and molecular packing

The internal structure of the self-assembled O-PDI and S-PDI has

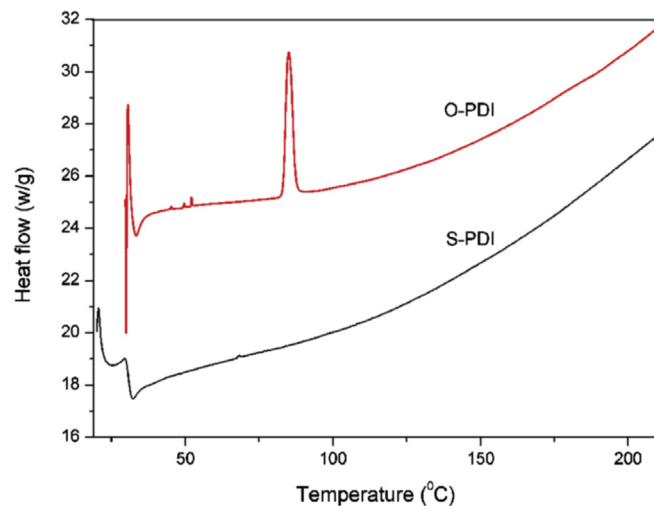


**Fig. 5.** DSC thermograms of O-PDI (red line) and S-PDI (black line) with heating rate of 10 °C/min under nitrogen condition. (For interpretation of the references to colour in this figure legend, the reader is referred to the web version of this article.)

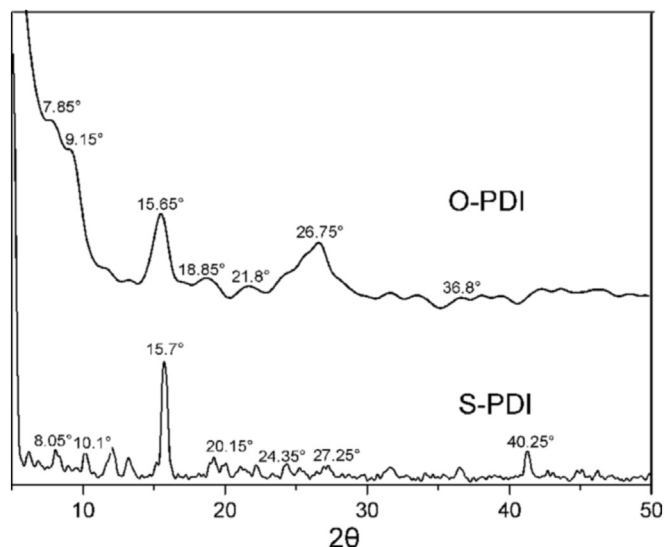


Fig. 6. X-ray diffraction analysis of the O-PDI and S-PDI.

been further investigated by performing X-ray diffraction (XRD) experiments (Fig. 6). The diffraction pattern is complicated and cannot be assigned completely. In the X-ray diffraction pattern of O-PDI, the peak at  $2\theta = 26.75^\circ$  ( $d$  spacing 3.3 Å) can be attributed to the  $\pi$ - $\pi$  stacking of the adjacent perylene because the distances of  $\pi$ - $\pi$  stacking between the perylene cores were approximately 3.5 Å [28,29]. The peak at approximately  $2\theta = 21.8^\circ$  ( $d$  spacing 4.03 Å) can be ascribed to the dislocation of  $\pi$ - $\pi$  stacking of perylene. Perylene derivatives are well known to exhibit a typical sharp diffraction peak at approximately  $8$ – $9^\circ$ , which is centered at a peak of  $7.85^\circ$  ( $d$  spacing 11.25 Å) [30]. Compared with O-PDI, the peak at  $7.85^\circ$  shifted to  $8.05^\circ$  with  $d$  space of 10.97 Å for S-PDI. The corresponding  $d$  spaces changed to 3.6 Å and 3.24 Å as the peaks shifted to  $24.35^\circ$  and  $27.25^\circ$  for S-PDI, respectively. The intensity of this diffraction peak decreases obviously for S-PDI. This result suggests that the  $\pi$ - $\pi$  stacking interactions of S-PDI units are weak, which is in good agreement with the optical properties. Additionally, X-ray powder diffraction measurement of O-PDI indicates a first diffraction peak

**Table 2**  
Calculated and experimental parameters for O-PDI, S-PDI and compound 1.

Molecule	HOMO <sup>a</sup>	LUMO <sup>a</sup>	$E_g^a$	$\lambda_{\max}$	$E_g^b$
O-PDI	-6.26	-3.62	2.64	510	2.43
S-PDI	-6.07	-3.40	2.67	500	2.48
Compound 1	-6.09	-3.62	2.47	525	2.36

<sup>a</sup> Calculated by DFT/B3LYP (in eV).

<sup>b</sup> At absorption maxima ( $E_g = 1240/\lambda_{\max}$ , in eV).

at  $2\theta = 9.15^\circ$  ( $d$  spacing 9.65 Å) with the second-order diffraction peak at  $2\theta = 18.85^\circ$  ( $d$  spacing 4.7 Å) and fourth order diffraction peak at  $2\theta = 36.8^\circ$  ( $d$  spacing 2.39 Å), and a group of similar diffraction peaks found in the same region for S-PDI are at  $10.1^\circ$  ( $d$  spacing 8.74 Å),  $20.15^\circ$  ( $d$  spacing 4.37 Å), and  $40.25^\circ$  ( $d$  spacing 2.19 Å). The first diffraction peak of O-PDI is assigned as (001) and the remaining higher order peaks as (00*l*) diffractions of the  $\alpha$ -form crystal as have been reported by Miyata [31]. A diffraction peak at  $2\theta = 15.65^\circ$  ( $d$  spacing 5.64 Å) is observed in the diffraction pattern of O-PDI, which is shifted to  $15.7^\circ$  ( $d$  spacing 5.62 Å) in the diffraction of S-PDI and can be attributed to the  $\alpha$ -form crystal also. The diffraction peak of S-PDI at about  $2\theta = 5.05^\circ$ , corresponding to a  $d$  space of about 1.73 nm, can be assigned to the length of the PDI units as shown in Fig. 2. The multiple orders of reflection indicate that the self-assembled structures are well-ordered and layered microstructures.

In order to check the effect of incorporating O/S heteroatom into the perylene skeleton quantum, chemical calculations were carried out with density functional theory (DFT) at the B3LYP/6-31G\* level. Fig. 7 shows the LUMO and the HOMO of O-PDI and S-PDI. One can note that the HOMO orbital of both O-PDI and S-PDI is centered on the perylene ring system, while the LUMO orbital is extended from the central perylene core to the heteroatom sites. The calculated molecular orbital (HOMO and LUMO) energies and experimental parameters are shown in Table 2. The molecular energy levels of the frontier molecular orbital revealed that the energy levels of HOMO and LUMO orbital as well as their energy gap can be tuned by the five-membered heterocyclic annulus. The energy level of the HOMO orbital for O-PDI is lowered relative to that of unsubstituted perylene diimide, while the energy level of the LUMO orbital is nearly unchanged. Moreover, the energy level of the HOMO orbital

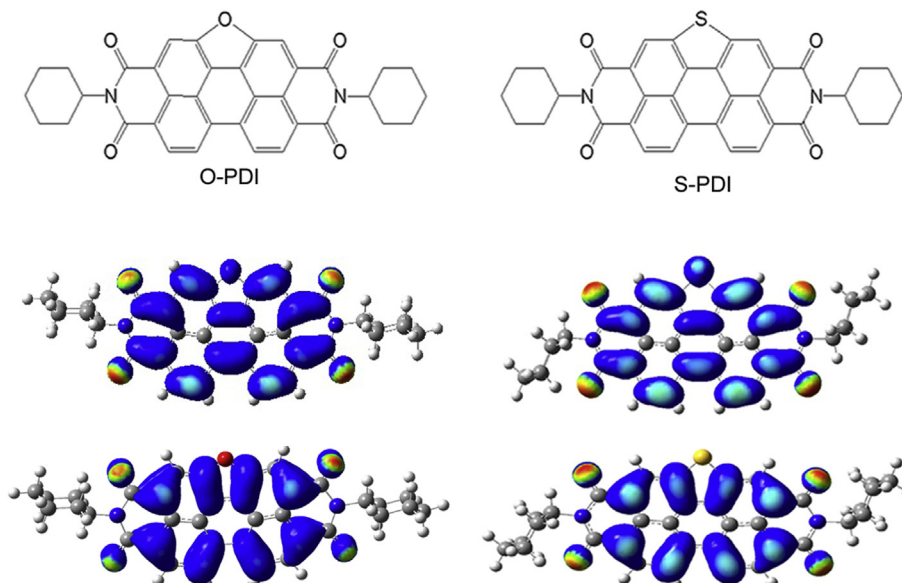
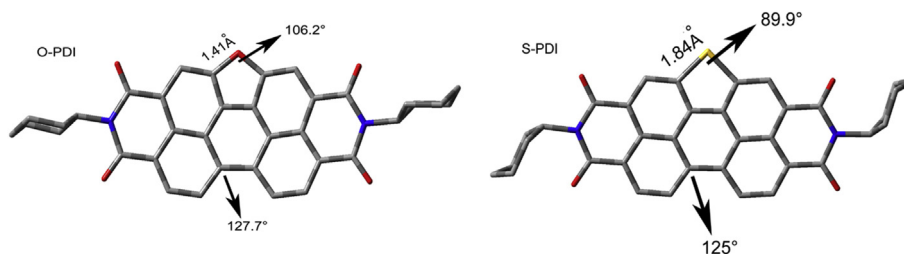


Fig. 7. Computed frontier orbitals of O-PDI and S-PDI. The upper graphs are the LUMOs and the lower ones are the HOMOs.



**Fig. 8.** Optimized structures of O-PDI and S-PDI obtained by DFT calculations at the B3LYP/6-31G\* level. The white, grey, blue, red, and yellow balls represent H, C, N, O, and S atoms, respectively. The H atoms are omitted for clarity. (For interpretation of the references to colour in this figure legend, the reader is referred to the web version of this article.)

for S-PDI is nearly unchanged. However, the energy level of the LUMO orbital is higher than that of unsubstituted perylene diimide. Therefore, the energy gap between HOMO and LUMO is enlarged for both O-PDI and S-PDI. This is consistent with the blue-shift of the electronic spectra for O-PDI and S-PDI in comparison with that of compound **1**. As expected, the HOMO-LUMO energy gap of S-PDI is higher than that of O-PDI, which is in good agreement with the electrochemical calculations. Optimized ground state geometric conformations of O-PDI and S-PDI are shown in Fig. 8. All molecules of the perylene skeleton and the heteroatom are of planar conformations. It is distinct that the formation of the five-membered ring induces the two naphthalene moieties to get close to each other in the site of the five-membered ring, while the two naphthalene moieties get far away in the site of the open ring. Moreover, the angles formed by CXC (X refers heteroatoms) and the bond length of C–X are 89.9° and 1.84 Å for S-PDI and 106.2° and 1.41 Å for O-PDI. As a whole, the core twist angle of S-PDI is smaller than that of O-PDI because of the bigger diameter of S atom than that of O atom.

Combining the results of X-ray diffraction, density functional theory (DFT) and the morphological analyses using TEM, the molecular arrangement in O-PDI/S-PDI crystal can be disclosed (Fig. 9 and Fig. S-7). The crystal structure of O-PDI exhibits a nearly planar molecular conformation with a packing arrangement consisting of edge-to-face dimers. The dimers adopt a almost herringbone packing arrangement with an interplanar distance of 3.3 Å which is similar to that in other perylene diimides crystals (about 3.5 Å) [32].

About twelve carbon atoms in perylene ring and one sulfur atom are close to the adjacent perylene ring (a perylene ring is composed of 20 carbon atoms) and the overlapping area is limited, indicating extraessential intermolecular  $\pi$ – $\pi$  actions in this case. S-PDI molecules remain the same face-to-face  $\pi$ – $\pi$  packing as all known crystal structures of perylene diimides. However, there is a huge transverse offset between adjacent S-PDI molecules, so that the overlapping area of successive  $\pi$ -conjugated perylene cores is small, and only eight carbon atoms in perylene ring and one sulfur atom are close to the adjacent perylene ring. This indicated more less-favored  $\pi$ -stacking than O-PDI. The interplanar distance between perylene moieties is found to be 3.23 Å. From the molecular modeling studies it can be established that the heteroatom has actually help firming up the stacking of the molecules through non-covalent bonding such as hydrogen bonds with H–O or H–S in CH<sub>3</sub>OH, electrostatic attraction between the electron-rich atom O/S and electron-poor perylene core. The short interplanar distance (3.3 Å for O-PDI and 3.23 Å for S-PDI) between perylene chromophores is favorable for the hopping transportation of charge carriers from one molecule to the neighboring molecule. Therefore, incorporating suitable heteroatom into the perylene skeleton can grant perylene diimide high mobility ensured by well-organized molecular packing with a short interplanar distance, and high solid-state luminescence efficiency through decreasing the intermolecular  $\pi$ – $\pi$  actions.

#### 4. Conclusions

In this study, we report O-PDI and S-PDI derivative that lack flexible solubilizing groups in the molecular structure, and demonstrate their self-assembly into nanoneedle and nanosheet, respectively. The heteroatom would help firming up the stacking of the molecules through non-covalent interactions, and electrostatic attraction between the electron-rich atom O/S and electron-poor perylene core. This study will be helpful for exploring feasible routes to acquire well defined organic nanostructures, and such molecular tailoring approach would be helpful for designing and synthesizing novel organic semiconductive materials with potential applications in electrically pumped lasers which require high emission efficiency when large current density is applied.

#### Acknowledgement

This work was supported by Provincial Natural Science Foundation of Shandong (ZR2012BM012).

#### Appendix A. Supplementary data

Supplementary data related to this article can be found at <http://dx.doi.org/10.1016/j.dyepig.2016.06.027>.

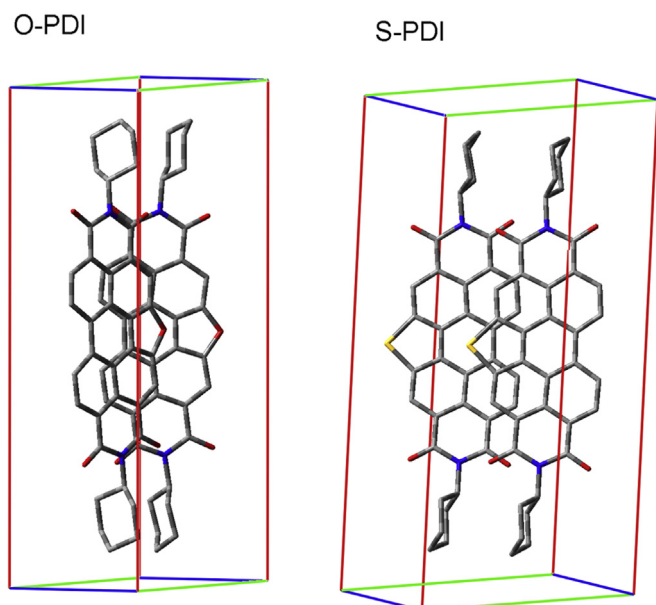


**Fig. 9.** View of the single crystal structure of O-PDI and S-PDI.

## References

- [1] Lehn JM. Toward self-organization and complex matter. *Science* 2002;295:2400–3.
- [2] Boobalan G, Imran P, Manoharan C, Nagarajan S. Fabrication of highly fluorescent perylene bisimide nanofibers through interfacial self-assembly. *J Colloid Interf Sci* 2013;393:377–83.
- [3] Boobalan G, Imran PM, Nagarajan S. Self-assembly, optical and electrical properties of fork-tailed perylene bisimides. *Superlattice Microstruct.* 2012;51:921–32.
- [4] Wasielewski MR. Energy, charge, and spin transport in molecules and self-assembled nanostructures inspired by photosynthesis. *J Org Chem* 2006;71:5051–66.
- [5] Boobalan G, Imran PM, Ramkumar SG, Nagarajan S. Fabrication of luminescent perylene bisimide nanorods. *J Lumin* 2014;146:146387–93.
- [6] Li C, Wonneberger H. Perylene imides for organic photovoltaics: yesterday, today, and tomorrow. *Adv Mater* 2012;24:613–36.
- [7] Tan WJ, Li X, Zhang JJ, Tian H. A photochromic diarylethene dyad based on perylene diimide. *Dyes Pigment* 2011;89:260–5.
- [8] Würthner F. Perylene bisimide dyes as versatile building blocks for functional supramolecular architectures. *Chem Commun* 2004;14:1564–79.
- [9] Xia YN, Yang PD, Sun YG, Wu YY, Mayers B, Gates B, et al. One-dimensional nanostructures: synthesis, characterization, and applications. *Adv Mater* 2003;15:353–89.
- [10] Dimitrakopoulos CD, Malenfant PRL. Organic thin film transistors for large area electronics. *Adv Mater* 2002;14:99–117.
- [11] Xiao K, Liu YQ, Qi T, Zhang W, Wang F, Gao JH, et al. A highly pi-stacked organic semiconductor for field-effect transistors based on linearly condensed pentathienoacene. *J Am Chem Soc* 2005;127:13281–6.
- [12] Li YJ, Liu TF, Liu HB, Tian MZ, Li YL. Self-assembly of intramolecular charge-transfer compounds into functional molecular systems. *ACC Chem Res* 2014;47:1186–98.
- [13] Zhao GJ, Han KL. Excited state electronic structures and photochemistry of heterocyclic annulated perylene (HAP) materials tuned by heteroatoms: S, Se, N, O, C, Si, and B. *J Phys Chem A* 2009;113:4788–94.
- [14] Qian HL, Liu CM, Wang ZH, Zhu DB. S-heterocyclic annulated perylene bisimide: synthesis and co-crystal with pyrene. *Chem Commun* 2006;44:4587–9.
- [15] Zhou Y, Liu W, Ma Y, Wang H, Qi L, Cao Y, et al. Single microwire transistors of oligoarenes by direct solution process. *J Am Chem Soc* 2007;129:12386–7.
- [16] Langhals H, Kirner S. Novel fluorescent dyes by the extension of the core of perylenetetracarboxylic bisimides. *Eur J Org Chem* 2000;2:365–80.
- [17] Li YJ, Liu TF, Liu HB, Tian MZ, Li YL. Self-assembly of intramolecular charge-transfer compounds into functional molecular systems. *Acc Chem Res* 2014;47:1186–98.
- [18] Muth MA, Carrasco Orozco M, Thelakkat M. Liquid-crystalline perylene diester polymers with tunable charge-carrier mobility. *Adv Funct Mater* 2011;21:4510–8.
- [19] Ma YS, Wang CH, Zhao YJ, Yu Y, Han CX, Qiu XJ, et al. Perylene diimide dyes aggregates: optical properties and packing behavior in solution and solid state. *Supramol Chem* 2007;19:141–9.
- [20] Chen KY, Chow TJ. 1,7-Dinitroperylene bisimides: facile synthesis and characterization as n-type organic semiconductors. *Tetrahedron Lett* 2010;51:5959–63.
- [21] Becke AD. Density-functional thermochemistry. III. The role of exact exchange. *J Phys Chem* 1993;98:5648–52.
- [22] Becke AD. Density-functional exchange-energy approximation with correct asymptotic behavior. *Phys Rev B* 1998;38:3098–100.
- [23] Ong KK, Jensen JO, Hameka HF. Theoretical studies of the infrared and Raman spectra of perylene. *J Mol Struct. Theochem* 1999;459:131–44.
- [24] Langhals H, Ismael R. Cyclophanes as model compounds for permanent, dynamic aggregates. Induced chirality with strong CD effects. *Eur J Org Chem* 1998;9:1915–7.
- [25] Funahashi M, Sonoda A. High electron mobility in a columnar phase of liquid-crystalline perylene tetracarboxylic bisimide bearing oligosiloxane chains. *J Mater Chem* 2012;22:25190–7.
- [26] Jiang W, Qian HL, Li Y, Wang ZH. Synthesis, photophysical properties, and solid-state packing arrangement. *J Org Chem* 2008;73:7369–72.
- [27] Locklin J, Li D, Mannsfeld SCB, Borkent EJ, Meng H, Advincula R, et al. Organic thin film transistors based on cyclohexyl-substituted organic semiconductors. *Chem Mater* 2005;17:3366–74.
- [28] Boom TV, Hayes RT, Zhao YY, Bushard PJ, Weiss EA, Wasielewski MR. Charge transport in photofunctional nanoparticles self-assembled from zinc 5, 10, 15, 20-tetrakis (perylene diimide) porphyrin building blocks. *J Am Chem Soc* 2002;124:9582–90.
- [29] Laschat S, Baro A, Steinke N, Giesselmann F, Hägele C, Scalia G. Discotic liquid crystals: from tailor-made synthesis to plastic electronics. *Angew Chem Int Ed* 2007;46:4832–87.
- [30] Ryong H, Chung EK, Hidetoshi O, Hitoshi K, Hachiro N. Effect of solvent on organic nanocrystal growth using the reprecipitation method. *J Cryst Growth* 2006;294:459–63.
- [31] Miyata T, Masuko T. Morphology of poly (l-lactide) solution-grown crystals. *Polymer* 1997;38:4003–9.
- [32] Shi MM, Tung VC, Nie JJ, Chen HZ, Yang Y. Bulky rigid substitutions: a route to high electron mobility and high solid-state luminescence efficiency of perylene diimide. *Org Electron* 2014;15:281–5.